

Targeting *Plasmodium falciparum*: Synthesis and evaluation of Phthalimide-HEA derivatives

Meenakshi Bansal^{1,2}, Brijesh Rathi^{2*}, Sumit Kumar^{1*}

¹Department of Chemistry, Deenbandhu Chhotu Ram, University of Science & Technology, Murthal, Sonapat Haryana 131039 India.

²HG Khorana Centre for Chemical Biology, Department of Chemistry, Hansraj College, University of Delhi, Delhi-110007 India.

Submitted on: 26-Sep-2024, Accepted and Published on: 08-Nov-2024

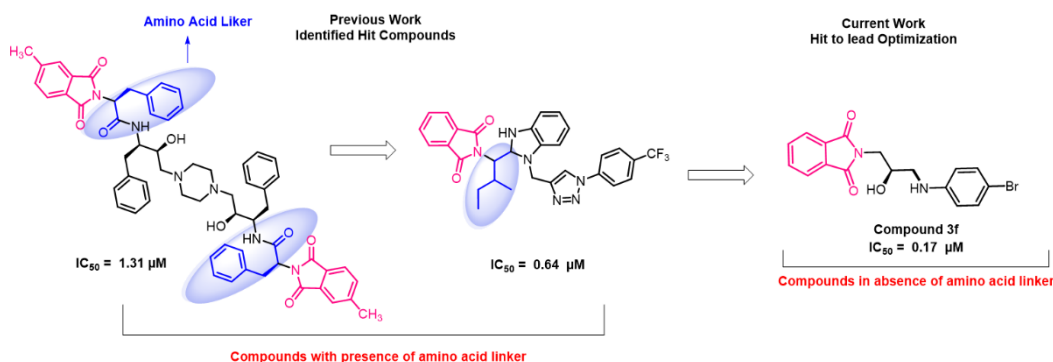
Article

ABSTRACT

We demonstrated a facile microwave-assisted synthesis of 16 novel phthalimide (Pht)-hydroxyethylamine (HEA)-based compounds isolated without tedious column

chromatography. Among all the tested compounds, **3b**, **3f**, and **3h** displayed 50% inhibitory concentration in the micromolar range (0.17 – 1.60 μM) against the 3D7 strain of *Plasmodium falciparum*. Compound **3f** showed the highest potency with an IC_{50} value of $0.17 \pm 0.001 \mu\text{M}$. Further, stage-specific assay revealed that hit **3f** was predominantly active at the ring stage. None of the compounds exhibited marked cytotoxicity up to 500 μM concentration on HepG2 liver cells, with cell viability range of 50–80%. Further, preliminary computational studies suggested that aminopeptidase N could be the potential target for hit **3f**, which needs to be validated through enzymatic assays.

Keywords: Hydroxyethylamine, Phthalimide, Malaria, Molecular Docking and MD Simulation



INTRODUCTION

One of the significant threats to human health in developing nations in Asia, Africa, and Latin America is parasitic illness.^{1,2} The tropical regions of these nations have a high parasite burden, and estimated yearly death records indicate the severity of these deadly diseases.³ According to the World Health Organization (WHO), nearly half of the global population is at risk and susceptible to parasitic diseases.⁴ At present, malaria remains a highly lethal parasitic disease transmitted by protozoan organisms that invade the human body, exerting a significant influence on public health.^{5,6}

Among the five species of malarial parasite, *Plasmodium falciparum* (Pf) is capable of inducing severe malaria syndromes and is responsible for the bulk of malaria-related deaths. The data presented in the World Malaria Report 2023 demonstrates that around 249 million estimated cases have been reported in 85

countries during the year 2022.^{7–9} Current treatment options to fight malaria are fast-acting medications, including artemisinin and its derivatives, *i.e.*, artemether, artesunate, and dihydroartemisinin (DHA), which typically eliminate the parasite within three days¹⁰. Among all the available treatment options, the most effective and widely used is first-line therapy, *i.e.*, artemisinin-based combination therapies (ACTs). However, the effectiveness of this widely acclaimed strategy is currently being jeopardized by the persistent establishment of resistance, which hinders the efficacy of treatment for patients. Despite the continuous and renewed push for malaria control interventions and well-established strategies, achieving complete malaria eradication remains a persistent challenge for public health organizations and researchers around the world.^{11–13} Furthermore, no highly effective vaccines are currently available for treatment. RTS, S/AS01 (Mosquirix™) is the sole vaccination that has demonstrated a positive response in clinical studies with poor efficacy (~36%).¹⁴ Hence, the discovery of novel compounds with unique mechanisms of action, targeting both established and emerging targets, is urgently necessary to effectively impede the spread of malaria.

Phthalimide (Pht)-based compounds have shown extensive potential in medicinal chemistry. Aside from many Pht-based

*Corresponding Author: Dr. Brijesh Rathi, PhD and Dr. Sumit Kumar, Ph.D.
Email: brijeshrathi@hrc.du.ac.in and sumitmalik.chem@dcrustm.org



FDA-approved drugs, recent reports have demonstrated the broad-spectrum biological properties of Pht against various diseases such as schistosomiasis¹⁵, malaria¹⁶, leishmaniasis¹⁷, tuberculosis¹⁸, and dengue.¹⁹ Pht also showed remarkable activity when hybridized with other significant pharmacophores, *i.e.*, triazole, piperazine, and thiazole. Vipam Kumar *et al.* are working extensively on Pht and similar classes of compounds and have discovered a few hits (**I-V**) over the past few years possessing high efficacy as antiplasmodial agents (Figure 1).²⁰⁻²⁴

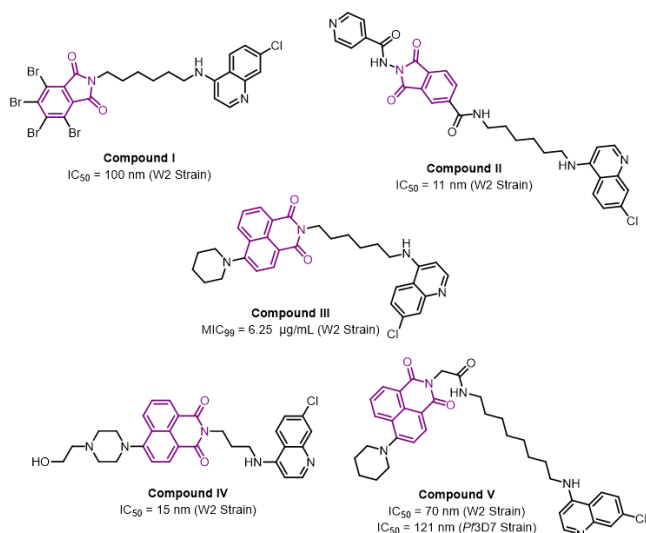


Figure 1. Previously reported Pht and similar class of hybrid compounds with good antiplasmodial efficacy.

Therefore, inspired by the literature and our ongoing work toward functionalizing the Pht scaffold, we synthesized 16 novel Hydroxyethyl Amine (HEA) compounds under microwave irradiation. The MW-assisted approach enabled the reaction to be completed within minutes/seconds with greatly improved yields under variable temperature ranges.^{25,26} Our group also optimized the MW-assisted ring-opening reaction in different solvents, including nitromethane.²⁷ This paper further optimized the reaction conditions, *i.e.*, time, temperature, and additives. All 16 compounds were evaluated for antiplasmodial efficacy along with the cytocompatibility assay.

RESULT AND DISCUSSION

Chemistry

Our team has previously developed Several Pht-HEA compounds that have demonstrated promising biological activity against the malaria parasite.²⁸⁻³⁰ Most compounds exhibited efficacy in the 1-5 μM range against the Pf3D7 strain. All the reported analogs were synthesized with an amino acid linker directly attached to the Pht moiety, forming an amide linkage with the HEA counterpart. However, a Pht and HEA moiety fusion is not explored without a linker. Therefore, to discover more potent compounds (hit-to-lead), we have explored the synthesis of Pht-HEA analogs without an amino acid linker (Figure 2).

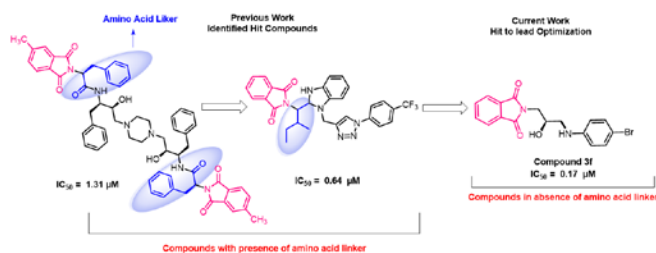


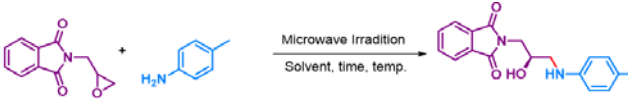
Figure 2. Hit-to-lead optimization of novel Pht-analogs as antiplasmodial agents.

Initially, we designed 16 analogs and evaluated their ADME profile using computational tools to understand the associated drug-likeness properties. The calculated parameters of the well-known rule of five (RO5) include (a) molecular weight, MW < 500 Da; (b) H-bond donors (nON < 5); (c) H-bond acceptors (nOHNH < 10); and (d) lipophilicity, log P predicted octanol/water partition coefficient (CLogP < 5). All the designed compounds displayed good physicochemical properties required for developing a drug molecule (Table S1; supporting information). The compounds were also evaluated for Drug-likeness model score (DrugL Score; -2 to +2 for drugability) and blood-brain Barrier (BBB) Score (0 indicates a low value, and 6 indicates a very high value). As per Weaver *et al.*,³¹ an optimal value of BBB protects the brain from the toxic side effects of therapeutic agents. However, at the same time, it is also crucial that medications developed for neurological disorders cross into the brain in therapeutic concentrations. Therefore, analysis of BBB interaction with designed compounds can lead to valuable and efficient drug design. All our designed compounds displayed an optimal BBB score, as neither showed a value < 2 nor > 5, predicating the non-harmful effect on the brain. Further, the compounds were analyzed for their drug-likeness score. Almost all compounds scored between the acceptable -2 to +2 range, with no Lipinski violation. Subsequently, the designed compounds were synthesized.

Pht-based epoxide synthesized³² and ring openings were carried out in the presence of substituted anilines as depicted in Scheme 1. We have explored the structure-activity relationship (SAR) through the various functional groups at aniline's *ortho*, *meta*, and *para* positions. Beforehand, we first decided to accelerate the ring-opening reaction; 2-(oxiran-2-ylmethyl) isoindoline-1,3-dione **1** was chosen as the starting substrate, and reaction conditions were optimized under microwave irradiation.²⁷ Generally, the opening step remains a time-consuming step for the synthesis of Pht-HEA analogs. Thus, we improved the ring-opening reaction step while performing it in various solvent systems under microwave irradiation, as described in Table 1. Our approach is consistent with the goals of modern chemists, who are trying to improve the efficiency of reactions involving dangerous chemicals by using safer, more environmentally friendly procedures. We screened various polar and non-polar solvents, such as dimethylsulphoxide (DMSO), acetonitrile (ACN), ethanol, dimethylformamide (DMF), toluene, nitromethane, isopropanol, and water at 75 °C (Table 1; entries 1-8).

Interestingly, all the solvents were ineffective in the reaction at 1 minute. Only ethanol offered a 22% yield of product **3a** with the recovery of starting material. Ethanol was used as a more environmentally friendly solvent than other organic solvents. This choice resulted in a notable enhancement in the yield (90%) of compound **3a** (entries 9-12) when the temperature was raised from 100-200 °C. We further optimized the reaction conditions and decreased the reaction time from 1 minute to 30 seconds at 200 °C, resulting in a 90% yield of **3a** with complete conversion of the starting material (entry 13). Notably, the optimized reaction conditions eliminate the need for purification *via* column chromatography, a time-consuming and expensive procedure.

Table 1. Optimization of reaction condition under microwave irradiation.^a

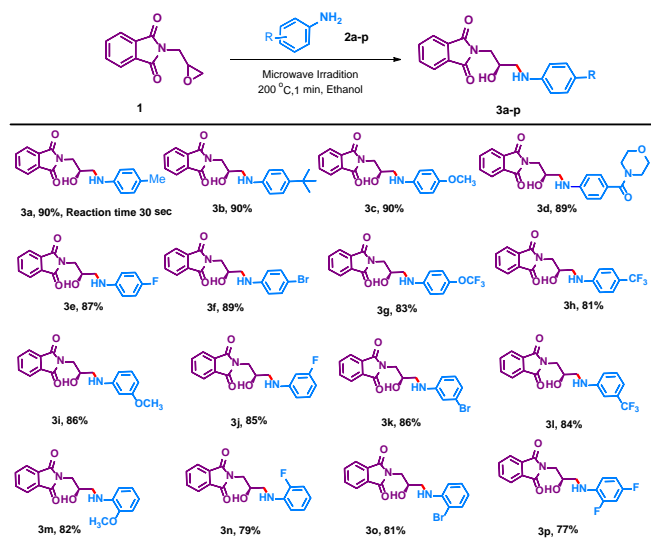


Entry No	Solvent	Time	Temp (°C)	Yield (%) ^b
1	ACN	1 min	75	n.r.
2	DMSO	1 min	75	12
3	DMF	1 min	75	n.r.
4	Toluene	1 min	75	n.r.
5	Nitromethane	1 min	75	13
6	Ethanol	1 min	75	22
7	Isopropanol	1 min	75	17
8	Water	1 min	75	n.r.
9	Ethanol	1 min	100	36
10	Ethanol	1 min	125	66
11	Ethanol	1 min	150	86
12	Ethanol	1 min	200	90
13	Ethanol	30 sec	200	90

^aReactions were performed using 1.0 mmol of compound **1** and 1.0 mmol of compound **2a** under microwave irradiation in 1.0 mL solvent. ^bIsolated yield; n.r. = No reaction.

Further, the substrate scope was extended for various substituted anilines, but we achieved better yield in 1 minute due to the lower nucleophilicity of anilines. Anilines with an electron donating group (EDG) at the para position, *i.e.*, -Me, -*t*Bu, and OCH₃, provide products **3a-c** in 90% yields. While the electron-withdrawing group (EWG), *i.e.*, -F, -Br, -OCF₃, and -CF₃, underwent the reaction to provide desired products **3e-h** in 81-89% yields, respectively. 3-Methoxyaniline reacted well to provide compound **3i** with an 86% yield. Electron-deficient anilines at *meta* position **2j-l** afforded the desired compounds **3j-l** with a comparable yield to the *para* position (84-86%).

Notably, *ortho*-substituted aniline **2m** -OCH₃ is well tolerated and offers the expected product of **3m** in 82% yield. It was noted that halogen-containing *ortho*-substituted anilines **2n-o** show a declining impact on yields of anticipated compounds **3n-o** (79-81%), possibly due to H-bonding in case of fluorine and steric hindrance in the case of bromine owing to its larger size.²⁷ In addition, 2,4-di-fluoroaniline **2p** was efficiently converted to the desired product **3p** in 77% yield.



Scheme 1. Scope of differently substituted anilines (**2a-p**) with the substrate (**1**) to deliver Pht and aniline-based analogs (**3a-p**). Reactions were performed using 1.0 mmol of **1** and 1.0 mmol of **2** at 200 °C under microwave irradiation in 1.0 mL ethanol in 1 min.

Biological Study

Evaluation of cytotoxicity, hemolytic activity, and antiplasmodial efficacy

Initially, the MTT assay assessed the cytotoxicity effect of synthesized compounds on the human liver cell line (HepG2). The compounds were evaluated at two different concentrations, 100 and 500 μM (Figure S51; supporting information). All the compounds exhibited a cell viability range of 50-80% at both tested concentrations after an incubation period of 48h. The assay result indicated that none of the compounds showed cytotoxic effects up to the 500 μM concentration.

A preliminary assessment was carried out to evaluate the antiplasmodial activity of the listed compounds (**3a-p**) towards the asynchronous *Pf* culture. Initial screening results were obtained at two different concentrations, *i.e.*, 1 μM and 5 μM against *Pf3D7* culture using SYBR Green assay. Tested compounds exhibited ~50% inhibition of the parasite at 5 μM concentration. The screening results are presented in Table 2, representing the results of two separate trials.

Table 2. *In vitro* efficacy against *Pf3D7* strain of malaria parasite of synthesized analogs.

Entry	Compound	% inhibition against <i>Pf3D7</i>	
		1 μM	5 μM
1	3a	45.31	>99
2	3b	59.72	>99
3	3c	40.39	>99
4	3d	49.77	98.18
5	3e	44.13	6.64
6	3f	79.10	89.79
7	3g	46.31	88.55
8	3h	53.54	84.76
9	3i	42.31	96.88
10	3j	42.98	83.92
11	3k	44.45	93.03
12	3l	42.41	94.82
13	3m	46.84	96.33
14	3n	33.00	77.78
15	3o	49.98	>99
16	3p	42.40	91.60

Further, to obtain SAR among the compounds, we have compared the results based on different functional groups at various positions. We compared the results for compounds (**3a-p**), where the most potent hits were **3f** (Table 2, entry 6), **3k** (Table 2, entry 11), and **3o** (Table 2, entry 15) containing Pht and HEA moiety with the combination of substituted anilines. Compound **3f** containing *para* bromo-substituted aniline displayed a potent 79.1% inhibition at 1 μ M while **3k** and **3o** possessing *meta* and *ortho*-substituted bromoaniline, showed 44.45% and 49.98% inhibition, respectively. This indicated the importance of *para* bromo-substitution on the aniline ring. Next, we also compared the presence of various functional groups at the *para* position, including compound **3e** (*para* -F substitution; 44.13% inhibition; Table 2, entry 5), **3g** (*para* -OCF₃ substitution; 46.31% inhibition; Table 2, entry 7), **3a** (*para* -CH₃ substitution; 45.31% inhibition; Table 2, entry 1), **3b** (*para* *tert*-butyl substitution; 44.13% inhibition; Table 2, entry 2), **3h** (*para* -CF₃ substitution; 53.54% inhibition; Table 2, entry 8), and **3c** (*para* -OCH₃ substitution; 40.39% inhibition; Table 2, entry 3). We found that the presence of any functional groups, whether EWG or EDG, does not yield better outcomes than the Bromo-substitution (**3f**) on the aniline ring at the *para* position.

Based on initial screening, a total of three compounds *viz.* **3b**, **3f**, and **3h** were selected for their IC₅₀ determination (Figure 3). In consideration of the preliminary screening outcomes, selected hit compounds underwent further screening to determine their inhibitory concentration at 50% (IC₅₀). Compounds **3b** and **3h** only show parasite reduction at higher concentrations, which is why a clear plateau was not visible in Figures 3A and 3C. Therefore, high concentrations are used to determine the resultant IC₅₀ values. Figure 3A represents the IC₅₀ curve for compound **3b**, exhibited an IC₅₀ value of $1.52 \pm 0.003 \mu$ M, **3f** showed a value of $0.17 \pm 0.001 \mu$ M (Figure 3B), and **3h** displayed $1.68 \pm 0.002 \mu$ M (Figure 3C). In general, compounds have shown low micromolar efficacy against *Pf*3D7, particularly compound **3f**, which is a very effective candidate.

Next, all the compounds were evaluated on red blood cells (RBCs) to assess their hemolytic activity. A hemolytic experiment was performed on RBC suspension with a volume fraction of 10%. The RBC suspension was treated with two doses (100 and 500 μ M) of all the listed compounds. Hemolysis was quantified at a wavelength of 500 nm (Figure S52; supplementary information) after an incubation period of 24h. The results indicated no substantial occurrence of hemolysis in RBCs up to 500 μ M concentrations.

Time-dependent and stage-specific assay

The success of antimalarial drugs centers on their ability to act rapidly and efficiently at various stages of the parasite's life cycle. We performed time-dependent experiments to examine the stage-specific activity of obtained hit **3f**. The sorbitol treatment synchronized the parasites at a stage when the culture included rings, trophs, and schizonts. After that, a growth inhibition assay was conducted against the *Pf*3D7 strain, and compounds **3f** and ART (positive control) were exposed to their respective IC₅₀ concentrations (0.17 μ M and 3 nM) and subjected to a closely synchronized culture incorporating ring stage (4% final

hematocrit and 1.5% parasitemia). Samples were initially taken at the first time point (**3h**) to make blood smears, followed by further collections at regular intervals of 3 hours (6, 9, 12h). Compounds **3f** displayed significant inhibition of the parasite growth compared to the untreated, with a 30-40% reduction in 12h post-treatment. The compound exhibited 40-60% inhibition when the study was extended up to 48h period. These results showed that compound **3f** is effective in the *Pf* ring stage (Figure 4A-B).

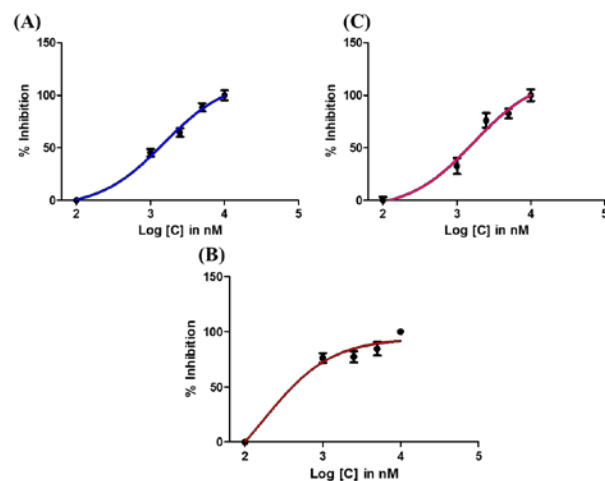


Figure 3. Graphical representation of IC₅₀ determination curves for hit analogs A) compound **3b**, B) compound **3f**, and C) compound **3h** show the IC₅₀ for aniline-based analogs.

During the stage-specific assessment, a similar 48h incubation was conducted for compounds at their respective IC₅₀ values, and the total percentages of different stages (rings, trophozoites, and schizonts) were counted and captured. To determine which stage is inhibited by the screened compounds, we compared the percentages of each stage in the control group with those in the compound-treated group. The parasite in the untreated control group exhibited regular growth patterns (*i.e.*, 74% rings, 6% trophozoites, and 20% schizonts), as depicted in Figure 4B. After treating the parasite with **3f**, the rings declined to 48%. In positive control ART, which is primarily active on the ring and early trophozoite stage, (the development from ring to trophs is

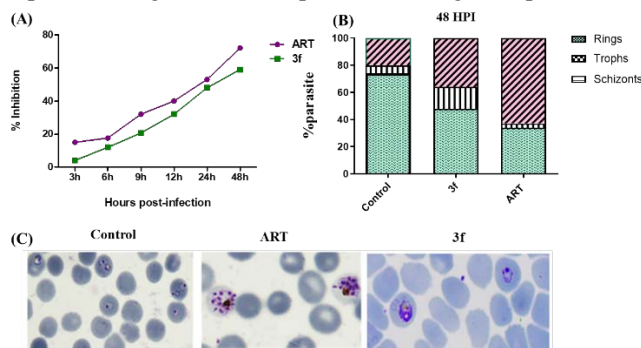


Figure 4. A) Growth progression evaluation of the complete growth cycle of the parasite at different time points, 3, 6, 9, 12, 24, and 48 h; B) Bar graphs showing % of rings, trophozoites, and schizonts at 48 h post-infection; and C) Giemsa-stained blood smear microscope images of control, ART and **3f** taken after 48 h post-infection.

hampered (34 % rings, 3% trophozoites, and 63% schizonts). Compared with the control group, the percentage of ring-stage parasites was reduced following treatment with compound **3f**. Nonetheless, compared with the control, no appreciable change was observed in the proportions of trophozoites and schizonts of parasites treated with **3f**. The morphological changes, including deformation in the ring and trophozoite stage, indicate the effect of **3f** on the parasite's growth, as shown in Figure 4C.

Computational Study

From the Uniprot database (accessed on May 15, 2023), we retrieved a complete list of 62 proteins, each of which was accompanied by its unique accession number (Table S2; supporting information). Additional analysis in PlasmoDB was conducted to get more information about the proteins of *Pf*. According to the results, a subset of 17 genes out of a total of 60 were determined to be essential (Figure S53; supporting information). This subset of genes was found to be necessary for parasite survival. Following that, the amino acid residues of these 17 proteins were analyzed to identify whether they are similar to proteins present in human beings. Only those proteins were selected for further study that displayed a percentage of identical residues lower than 30.0% with humans.³³ proteins with a query coverage below 55% were also included.³⁴ Four proteins were excluded from the analysis due to their structural similarity, resulting in a remaining set of 13 proteins that were subsequently examined for their structural availability. This study assessed the accessibility of crystal structures or protein models generated by alpha fold for the 13 investigated proteins. Structural information was obtained for all the proteins except for eukaryotic translation initiation factor 2- α kinase PK4 (UniProt accession no. C6KTB8), for which no structural data was available in either crystal or model form.

Table 3. Site-specific docking depicting Docking Score, XP Gscore, and Binding free energy (MMGBSA dG Blind; ΔG) are indicated in Kcal/mol along with blind docking results (N-: negative and P+: Positive)

S. No.	Protein	Docking Score	XP Gscore	ΔG	Blind
1	Ubiquitin carboxyl-terminal hydrolase UCH54	-4.769	-4.769	-52.32	N-
2	Bifunctional glucose-6-phosphate 1-dehydrogenase/6-phosphogluconolactonase	-2.538	-2.538	-34.86	N-
3	Plasmeprin IX	-7.141	-7.141	-56.58	N-
4	Aminopeptidase N	-6.178	-6.178	-45.21	P+
5	Leucine aminopeptidase	-6.025	-6.025	-47.31	P+
6	Dual specificity protein phosphatase YVH1	-5.776	-5.776	-58.61	N-
7	Falcilysin	-4.936	-4.936	-38.02	N-
8	Calcium-dependent protein kinase 5	-4.832	-4.832	-45.90	N-
9	DNA-endonuclease	-3.923	-3.923	-26.09	N-
10	Plasmeprin V	-6.751	-6.751	-55.63	P+
11	Serine-repeat antigen protein 5	-3.681	-3.681	-39.01	P+

Next, molecular docking^{35,36} was conducted to investigate the binding affinity identified hits **3f** with 12 proteins, as outlined in Table 3. The obtained results were additionally validated through blind docking. The compounds **3f** exhibited binding affinity against four proteins, and results indicated that it predominately displayed better binding interaction with aminopeptidase N (Table 3, entry 4), leucine aminopeptidase (Table 3, entry 5), and Plm V (Table 1, entry 10). These protein targets were validated through molecular blind docking studies; however, **3f** also showed positive results for serine-repeat antigen protein 5 (Table 1, entry 11) during blind docking; unfortunately, the docking score was significantly lower than other validated proteins. Therefore, the binding interaction analysis for compound **3f** was analyzed against three proteins (aminopeptidase N, leucine aminopeptidase, and Plm V).

Furthermore, in the context of binding interactions and molecular dynamics (MD) simulation studies, we analyzed the results for compound **3f** with Plm V and Leucine aminopeptidase. During the molecular dynamics (MD) simulation, it was noted that the complexes of compound **3f** with Plm V and leucine aminopeptidase were inherently unstable. As a result, MD simulations for these complexes were not conducted for the intended simulation duration of 100 ns. The complex for **3f**-leucine aminopeptidase moved out of the trajectory after a simulation period of 20 ns (Figure S54; supporting information). However, the **3f**-Plm V complex moved out after 40 ns, as illustrated in Figure S55; supporting information). Interestingly, the targeted MD simulation period of 100 ns was successfully achieved for the **3f**-aminopeptidase N complex, and it demonstrated good stability throughout the entire duration (Figure 5).

Extensive computational studies have indicated that compound **3f** could be specific for aminopeptidase N; however, further validation studies are essential before reaching any conclusion.

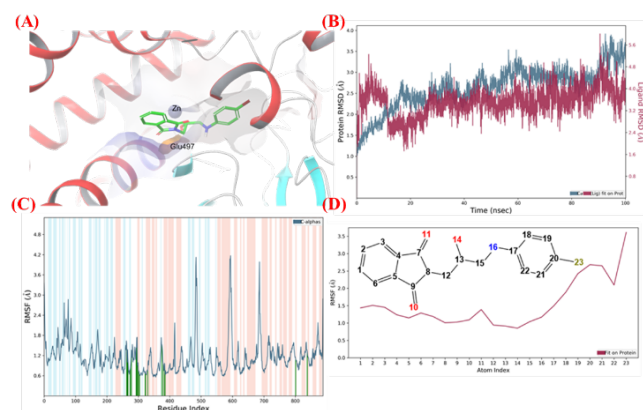


Figure 5. A) Schematic depiction of the three-dimensional structure of docking outputs against Plm IX for compound **3f**; B) The outcomes of a molecular dynamics (MD) simulation lasting 100 nanoseconds (ns). It reports Root Mean Square Deviations (RMSD) values obtained from the protein structure (3EBH) with compound **3f**. The graph depicts the RMSD value of the ligand (represented by the purple line) from the protein backbone (represented by the blue line); C) The root mean square fluctuation (RMSF) was calculated for the protein α -carbon in complex with **3f** ligand (pink band); α -

helix, blue band: beta-sheet, white band: loop, green lines: residue interacted with **3f**; and D) Ligand RMSF of **3f** in complex with 3EBH protein.

EXPERIMENTAL

Chemistry

The chemicals and solvents used in the experiment were not purified before use and were purchased from reliable suppliers such as GLR, TCI, and Sigma Aldrich. To ensure the purity of the synthesized chemicals, thin-layer chromatography (TLC) analysis was carried out using 60 F254 silica gel plates from Sigma-Merck. The microwave reactions were conducted using controlled temperature programming using the "Anton Paar Microwave Reactor: Monowave 400". Tetramethylsilane was used as an internal standard, and CDCl₃ and DMSO were used as the solvents in the NMR spectroscopy analysis. The shifts (δ) and coupling constants (J) were reported in parts per million (ppm) and Hz, respectively. Reverse-phase HPLC studies were performed to determine the purity of the compounds. The HPLC system used was Gilson, USA, which had an analytical column (C18), a Thermo Separation Spectra SERIES UV100 detector, and software. The mobile phase used for purification analysis was a mixture of acetonitrile and water (v/v).

General procedure for the synthesis of Pht analogs (3a-p)

For the synthesis of Pht analogs, we slightly modified the reported procedure²⁷ to obtain the products with high yields. In a 30 mL pressure seal, 2-(oxiran-2-ylmethyl)isoindoline-1,3-dione (**1**) (1.0 mmol), primary amines (**2a-p**) (1.0 mmol), ethanol (1 mL) were taken heated under microwave at 200 °C for 1.0 minutes. The completion of the reaction was monitored by thin-layer chromatography. After completion of the reaction, the contents were transferred to a 100 mL round bottom flask, and ethanol was removed under reduced pressure. The crude product was extracted with ethyl acetate (20 mL x 3) and brine solution (10 mL x 3). The organic layer was separated and dried over anhydrous sodium sulfate. Ethyl acetate was concentrated on a rotary evaporator, and the products were isolated in pure form **3a-p**. The obtained compounds were purified with hexane (5 mL x 2). ¹H NMR, ¹³C NMR, and HR-MS techniques confirmed the chemical composition.

Spectroscopic Data

(R)-2-(2-hydroxy-3-(p-tolylamino)propyl)isoindoline-1,3-dione (3a). yield, 90%; mp. 124-126 °C; ¹H NMR (400 MHz, CDCl₃) δ 7.86 (dd, J = 5.2, 3.1 Hz, 2H, H-1), 7.73 (dd, J = 5.2, 3.1 Hz, 2H, H-1'), 6.98 (d, J = 8.0 Hz, 2H, H-2), 6.60 (d, J = 8.1 Hz, 2H, H-3), 4.18 – 4.13 (m, 1H, H-5), 3.95 – 3.83 (m, 2H, H-6 and 6'), 3.27 (dd, J = 13.2, 4.7 Hz, 1H, H-7), 3.16 (dd, J = 13.2, 6.8 Hz, 1H, H-7'), 2.23 (s, 3H, H-8). ¹³C-NMR (100 MHz, CDCl₃) δ 169.0 (C=O), 145.7 (*Ar*-NH), 134.3 (C-1), 131.9 (C-1a), 129.6 (C-2), 127.3 (C-1'), 123.6 (*Ar*), 113.6 (*Ar*), 68.9 (C-5), 47.9 (C-7), 42.1 (C-6), 20.4 (C-8). HRMS calcd. (M+H) for C₁₈H₁₈N₂O₃ 311.1390; found 311.1387.

(R)-2-(3-((4-*tert*-butyl)phenyl)amino)-2-hydroxypropyl)isoindoline-1,3-dione (3b). yield, 90%; mp. 107-109 °C; ¹H-NMR (400 MHz, CDCl₃) δ 7.85 (dd, J = 5.4, 3.1 Hz, 2H, H-1), 7.73 (dd, J = 5.5, 3.0 Hz, 2H, H-1'), 7.20 (d, J = 8.7 Hz, 2H, H-2), 6.64 (d, J = 8.7 Hz, 2H, H-3), 4.20 – 4.11

(m, 1H, H-5), 3.93 – 3.83 (m, 2H, H-6 and 6'), 3.28 (dd, J = 13.2, 4.8 Hz, 1H, H-7), 3.17 (dd, J = 13.2, 6.8 Hz, 1H, H-7'), 1.27 (s, 9H, H-8). ¹³C-NMR (100 MHz, CDCl₃) δ 169.1 (C=O), 145.7 (*Ar*-NH), 140.8 (*Ar*), 134.3 (C-1), 131.9 (C-1a), 126.1 (C-1'), 123.6 (C-2), 113.1 (C-3), 68.8 (C-5), 47.7 (C-7), 42.1 (C-6), 33.9 (C-8), 31.6 (*C-tert*-butyl). HRMS calcd. (M+H) for C₂₁H₂₄N₂O₃ 353.1820; found 353.1855.

(R)-2-(2-hydroxy-3-((4-methoxyphenyl)amino)propyl)isoindoline-1,3-dione (3c). yield, 90%; mp. 158-160 °C; ¹H-NMR (400 MHz, CDCl₃) δ 7.86 (dd, J = 5.5, 3.0 Hz, 2H, H-1), 7.73 (dd, J = 5.4, 3.1 Hz, 2H, H-1'), 6.77 (d, J = 8.9 Hz, 2H, H-2), 6.64 (d, J = 8.9 Hz, 2H, H-3), 4.17 – 4.11 (m, 1H, H-5), 3.91 – 3.88 (m, 2H, H-6 and 6'), 3.74 (s, 3H, H-8), 3.24 (dd, J = 13.0, 4.6 Hz, 1H, H-7), 3.12 (dd, J = 13.0, 6.9 Hz, 1H, H-7'). ¹³C-NMR (100 MHz, CDCl₃) δ 169.0 (C=O), 152.6 (*Ar*-OCH₃), 142.2 (*Ar*-NH), 134.3 (C-1), 131.9 (C-1a), 123.6 (C-1'), 114.9 (*Ar*), 68.9 (C-5), 55.8 (C-8), 48.7 (C-7), 42.2 (C-6). HRMS calcd. (M+H) for C₁₈H₁₈N₂O₄ 327.1300; found 327.1334.

(R)-2-(2-hydroxy-3-((4-(morpholine-4-carbonyl)phenyl)amino)propyl)isoindoline-1,3-dione (3d). yield, 89%; mp. 167-169 °C; ¹H NMR (400 MHz, CDCl₃) δ 7.79 (dd, J = 5.5, 3.4 Hz, 2H, H-1), 7.62 (d, J = 7.5 Hz, 2H, H-3), 7.58 (dd, J = 5.5, 3.4 Hz, 2H H-2), 6.60 (d, J = 7.5 Hz, 2H, H-4), 4.72 (s, 1H, OH), 4.31 – 4.26 (m, 1H, H-5), 3.88 (dd, J = 12.5, 2.2 Hz, 1H, H-6), 3.79 – 3.51 (m, 9H, H-6, 7 and 8), 3.37 (dd, J = 12.4, 2.3 Hz, 1H, H-9), 3.12 (dd, J = 12.4, 2.3 Hz, 1H, H-9). ¹³C NMR (100 MHz, CDCl₃) δ 171.1 (C-4a), 169.1 (C=O), 149.8 (C-3a), 134.3 (C-1), 131.9 (C-1a), 129.5 (C-4), 123.6 (C-3b), 123.3 (C-2), 114.2 (C-3), 112.2 (C-3), 68.6 (C-5), 67.1 (C-8 and 9), 46.8 (C-7), 42.1 (C-6). HRMS calcd. (M+H) for C₂₂H₂₃N₃O₅ 410.1710; found 410.1714.

(R)-2-(3-((4-fluorophenyl)amino)-2-hydroxypropyl)isoindoline-1,3-dione (3e). yield, 87%; mp. 156-158 °C; ¹H-NMR (400 MHz, CDCl₃) δ 7.86 (dd, J = 5.6, 3.1 Hz, 2H, H-1), 7.74 (dd, J = 5.6, 3.1 Hz, 2H, H-1'), 6.94 – 6.81 (m, 2H, H-3), 6.66 – 6.53 (m, 2H, H-2), 4.22 – 4.08 (m, 1H, H-5), 3.94 – 3.86 (m, 2H, H-6 and 6'), 3.26 – 3.10 (m, 2H, H-7 and 7'). ¹³C-NMR (101 MHz, CDCl₃) δ 169.1, 144.3 (d, J = 234.7 Hz, 1C, *Ar*), 134.4 (d, J = 32.1 Hz, 1C, *Ar*), 131.8 (C-1), 123.6 (C-1'), 115.9 (C-3), 115.7 (*Ar*) (d, J = 22.9 Hz, 1C, *Ar*), 114.3 (*Ar*), 68.9 (C-5), 48.2 (C-7), 42.2 (C-6). HRMS calcd. (M+H) for C₁₇H₁₅FN₂O₃ 315.1139; found 315.1141.

(R)-2-(3-((4-bromophenyl) amino)-2-hydroxypropyl)isoindoline-1,3-dione (3f). yield, 89%; mp. 178-180 °C; ¹H-NMR (400 MHz, DMSO-*d*₆) δ 7.83 – 7.78 (m, 4H, H-1 and 1'), 7.14 (d, J = 8.9 Hz, 2H, H-2), 6.53 (d, J = 9.0 Hz, 2H, H-3), 5.13 (d, J = 5.3 Hz, 1H, OH or H-4), 4.01 – 3.88 (m, 1H, H-5), 3.64 – 3.58 (m, 1H, H-6), 3.58 – 3.52 (m, 1H, H-6'), 3.15 – 3.04 (m, 1H, H-7), 3.01 – 2.90 (m, 1H, H-7'). ¹³C-NMR (100 MHz, DMSO-*d*₆) δ 168.6 (C=O), 148.6 (*Ar*-NH), 134.7 (C-2), 132.3 (C-1a), 131.8 (C-1), 123.4 (C-1'), 114.6 (C-3), 106.7 (*Ar*-Br), 66.8 (C-5), 47.7 (C-7), 42.9 (C-6). HRMS calcd. (M+H) for C₁₇H₁₅BrN₂O₃ 375.0339; found 375.0346.

(R)-2-(2-hydroxy-3-((4-(trifluoromethoxy)phenyl)amino)propyl)isoindoline-1,3-

dione (3g). yield, 83%; mp. 182-184 °C; ¹H-NMR (400 MHz, DMSO-d₆) δ 7.85 – 7.77 (m, 4H, H-1 and 1'), 7.00 (d, *J* = 9.0 Hz, 2H, H-2), 6.61 (d, *J* = 9.1 Hz, 2H, H-3), 5.15 (d, *J* = 5.3 Hz, 1H, H-4), 4.02 – 3.91 (m, 1H, H-5), 3.68 – 3.51 (m, 2H, H-6 and 6'), 3.18 – 3.06 (m, 1H, H-7), 3.02 – 2.91 (m, 1H, H-7'). ¹³C-NMR (100 MHz, DMSO-d₆) δ 168.6 (C=O), 148.6 (*Ar*), 138.8 (*Ar*), 134.7 (*Ar*), 132.3 (C-1), 123.4 (C-1'), 122.5 (*Ar*), 112.9 (*Ar*), 66.8 (C-5), 47.8 (C-7), 42.9 (C-6). HRMS calcd. (M+H) for C₁₈H₁₅F₃N₂O₄ 381.1017; found 381.1058.

(R)-2-(2-hydroxy-3-((4-(trifluoromethyl)phenyl)amino)propyl)isoindoline-1,3-dione (3h). yield, 81%; mp. 210-212 °C; ¹H-NMR (400 MHz, CDCl₃) δ 7.88 (dd, *J* = 5.5, 3.0 Hz, 2H, H-1), 7.76 (dd, *J* = 5.4, 3.1 Hz, 2H, H-1'), 7.39 (d, *J* = 8.5 Hz, 2H, H-2), 6.67 (d, *J* = 8.4 Hz, 2H, H-3), 4.20 – 4.14 (m, 1H, H-5), 3.93 (d, *J* = 4.9 Hz, 2H, H-6 and 6'), 3.32 – 3.21 (m, 2H, H-7 and 7'). ¹³C-NMR (100 MHz, DMSO-d₆) δ 169.4 (C=O), 153.0 (*Ar*-NH), 135.5 (C-1), 133.0 (C-1a), 127.4 (C-8), 124.2 (C-1'), 116.3 (*Ar*), 112.7 (*Ar*), 67.5 (C-5), 48.0 (C-7), 43.5 (C-6). HRMS calcd. (M+H) for C₁₈H₁₅F₃N₂O₃ 365.1108; found 365.1111.

(R)-2-(2-hydroxy-3-((3-methoxyphenyl)amino)propyl)isoindoline-1,3-dione (3i). yield, 86%; mp. 96-98 °C; ¹H NMR (400 MHz, CDCl₃) δ 7.84 (dd, *J* = 5.4, 3.1 Hz, 2H, H-1), 7.72 (dd, *J* = 5.4, 3.1 Hz, 2H, H-1'), 7.05 (t, *J* = 8.1 Hz, 1H, H-2), 6.27 (dd, *J* = 8.1, 2.2 Hz, 2H, H-3), 6.20 (t, *J* = 2.2 Hz, 1H, H-2'), 4.19 – 4.10 (m, 1H, H-5), 3.88 (dd, *J* = 5.1, 3.8 Hz, 2H, H-6 and 6'), 3.74 (s, 3H, H-8), 3.25 (dd, *J* = 13.3, 4.9 Hz, 1H, H-7), 3.16 (dd, *J* = 13.3, 6.8 Hz, 1H, H-7'). ¹³C NMR (100 MHz, CDCl₃) δ 169.1 (C=O), 160.9 (*Ar*-OCH₃), 149.4 (*Ar*-NH), 134.3 (C-1), 131.9 (C-1a), 130.1 (*Ar*), 123.6 (C-1'), 106.35 (*Ar*), 103.2 (*Ar*), 99.3 (*Ar*), 68.9 (C-5), 55.1 (C-8), 47.4 (C-7), 42.1 (C-6). HRMS calcd. (M+H) for C₁₈H₁₅F₃N₂O₃ 327.1300; found 327.1335.

(R)-2-(3-((3-fluorophenyl)amino)-2-hydroxypropyl)isoindoline-1,3-dione (3j). yield, 85%; mp. 166-168 °C; ¹H-NMR (400 MHz, DMSO-d₆) δ 7.89 – 7.81 (m, 4H, H-1 and 1'), 6.99 (t, *J* = 8.0 Hz, 1H, H-2), 6.77 (t, *J* = 2.0 Hz, 2H, H-3), 6.69 – 6.56 (m, 1H, *Ar*), 5.19 (d, *J* = 5.2 Hz, 1H, H-4), 4.05 – 3.91 (m, 1H, H-5), 3.68 – 3.57 (m, 2H, H-6 and 6'), 3.21 – 3.10 (m, 1H, H-7), 3.07 – 2.95 (m, 1H, H-7'). ¹³C-NMR (100 MHz, DMSO-d₆) δ 168.6 (C=O), 165.2 (d, *J* = 241.3 Hz, 1C, *Ar*), 151.5 (*Ar*-NH), 134.7 (d, *J* = 10.8 Hz, 1C, *Ar*), 132.3 (C-1'), 130.6 (C-1a), 123.4 (d, *J* = 7.2 Hz, 1C, *Ar*), 108.9 (*Ar*), 102.0 (*Ar*), 66.8 (C-5), 47.6 (C-7), 42.8 (C-6). HRMS calcd. (M+H) for C₁₇H₁₅FN₂O₃ 315.1100; found 315.1148.

(R)-2-(3-((3-bromophenyl)amino)-2-hydroxypropyl)isoindoline-1,3-dione (3k). yield, 86%; mp. 187-189 °C; ¹H-NMR (400 MHz, DMSO-d₆) δ 7.89 – 7.81 (m, 4H, H-1 and 1'), 6.99 (t, *J* = 8.0 Hz, 1H, H-2), 6.77 (t, *J* = 2.0 Hz, 1H, H-2'), 6.69 – 6.56 (m, 2H, H-3), 5.19 (d, *J* = 5.2 Hz, 1H, H-4), 4.05 – 3.91 (m, 1H, H-5), 3.68 – 3.10 (m, 2H, H-6 and 6'), 3.21 – 3.10 (m, 1H, H-7), 3.07 – 2.95 (m, 1H, H-7'). ¹³C-NMR (100 MHz, CDCl₃) δ 169.6 (C=O), 151.1 (*Ar*-NH), 134.8 (C-1), 132.3 (C-1a), 131.1 (C-2'), 123.4 (C-1'), 122.9 (*Ar*-Br), 118.4 (C-2), 114.6 (C-3), 111.7 (C-3), 66.8 (C-5), 47.5 (C-7), 42.8 (C-

6). HRMS calcd. (M+H) for C₁₇H₁₅BrN₂O₃ 375.0339; found 375.0343.

(R)-2-(2-hydroxy-3-((3-(trifluoromethyl)phenyl)amino)propyl)isoindoline-1,3-dione (3l). yield, 84%; mp. 209-211 °C; ¹H-NMR (400 MHz, DMSO-d₆) δ 7.88 – 7.81 (m, 4H, H-1 and 1'), 7.26 (t, *J* = 7.8 Hz, 1H, *Ar*), 6.87 (d, *J* = 7.2 Hz, 2H, *Ar*), 6.79 (d, *J* = 7.8 Hz, 1H, *Ar*), 5.22 (d, *J* = 5.2 Hz, 1H, H-4), 4.06 – 3.95 (m, 1H, H-5), 3.71 – 3.57 (m, 2H, H-6 and 6'), 3.26 – 3.18 (m, 1H, H-7), 3.11 – 3.02 (m, 1H, H-7'). ¹³C-NMR (100 MHz, DMSO-d₆) δ 169.3 (C=O), 150.6 (*Ar*), 135.5 (*Ar*), 133.0 (C-1), 131.0 (*Ar*), 124.1 (C-1'), 116.8 (*Ar*), 112.7 (*Ar*), 109.1, 67.5 (C-5), 48.2 (C-7), 43.6 (C-6). HRMS calcd. (M+H) for C₁₈H₁₅F₃N₂O₃ 365.1108; found 365.1110.

(R)-2-(2-hydroxy-3-((2-methoxyphenyl)amino)propyl)isoindoline-1,3-dione (3m). yield, 82%; mp. 102-104 °C; ¹H-NMR (400 MHz, CDCl₃) δ 7.85 (dd, *J* = 5.4, 3.1 Hz, 2H, H-1), 7.72 (dd, *J* = 5.4, 3.1 Hz, 2H, H-1'), 6.89 – 6.80 (m, 1H, H-2), 6.78 – 6.72 (m, 1H, H-2'), 6.70 – 6.63 (m, 2H, H-3), 4.22 – 4.12 (m, 1H, H-5), 3.92 – 3.87 (m, 2H, H-6 and 6'), 3.83 (s, 3H, H-8), 3.31 (dd, *J* = 13.3, 4.6 Hz, 1H, H-7), 3.19 (dd, *J* = 13.3, 7.0 Hz, 1H, H-7'). ¹³C-NMR (100 MHz, CDCl₃) δ 169.0 (C=O), 147.2 (*Ar*-OCH₃), 137.9 (*Ar*-NH), 134.3 (C-1) 131.9 (C-1a), 123.6 (C-1'), 121.3 (C-3), 117.2 (C-3), 110.4 (C-2), 109.6 (C-2'), 69.0 (C-5), 55.5 (C-8), 47.5 (C-7), 42.2 (C-6). HRMS calcd. (M+H) for C₁₈H₁₈N₂O₄ 327.1300; found 327.1335.

(R)-2-(3-((2-fluorophenyl)amino)-2-hydroxypropyl)isoindoline-1,3-dione (3n). yield, 79%; mp. 131-132 °C; ¹H-NMR (400 MHz, CDCl₃) δ 7.85 (dd, *J* = 5.5, 3.0 Hz, 2H, H-1), 7.73 (dd, *J* = 5.5, 3.0 Hz, 2H, H-1'), 7.01 – 6.90 (m, 2H, H-2), 6.74 – 6.72 (m, 1H, H-3), 6.65 – 6.60 (m, 1H, H-3'), 4.23 – 4.13 (m, 1H, H-5), 3.94 – 3.88 (m, 2H, H-6 and 6'), 3.32 (dd, *J* = 13.3, 4.8 Hz, 1H, H-7), 3.21 (dd, *J* = 13.3, 7.0 Hz, 1H, H-7'). ¹³C-NMR (100 MHz, CDCl₃) δ 169.1 (C=O), 153.1 (d, *J* = 236.4 Hz, 1C, *Ar*-F), 136.4 (d, *J* = 11.1 Hz, 1C, *Ar*-NH), 134.3 (C-1), 131.8 (C-1a), 124.6 (C-1'), 123.6 (*Ar*), 117.2 (d, *J* = 6.9 Hz, 1C, *Ar*), 114.5 (*Ar*), 112.5 (*Ar*), 68.9 (C-5), 47.1 (C-7), 42.1 (C-6). HRMS calcd. (M+H) for C₁₇H₁₅FN₂O₃ 315.1100; found 311.1141.

(R)-2-(3-((2-bromophenyl)amino)-2-hydroxypropyl)isoindoline-1,3-dione (3o). yield, 81%; mp. 92-94 °C; ¹H NMR (400 MHz, CDCl₃) δ 7.85 – 7.78 (m, 4H, H-1 and 1'), 7.36 (dd, *J* = 7.9, 1.5 Hz, 1H, H-2), 7.18 – 7.09 (m, 1H, H-2'), 6.70 (dd, *J* = 8.2, 1.3 Hz, 1H, H-3), 6.53 – 6.46 (m, 1H, H-3'), 5.35 (d, *J* = 5.3 Hz, 1H, H-4), 4.02 – 3.96 (m, 1H, H-5), 3.68 – 3.56 (m, 2H, H-6 and 6'), 3.28 – 3.22 (m, 1H, H-7), 3.09 – 2.99 (m, 1H, H-7'). ¹³C NMR (101 MHz, CDCl₃) δ 168.6 (C=O), 145.5 (*Ar*-NH), 134.8 (C-3), 132.6 (C-1), 132.3 (C-1a), 129.1 (C-2'), 123.4 (C-1'), 117.9 (C-2), 112.2 (C-3), 109.2 (*Ar*-Br), 66.6 (C-5), 47.3 (C-7), 42.5 (C-6). HRMS calcd. (M+H) for C₁₇H₁₅BrN₂O₃ 375.0339; found 375.0349.

2-(3-((2,4-difluorophenyl)amino)-2-hydroxypropyl)isoindoline-1,3-dione (3p). yield, 77%; mp. 137-139 °C; ¹H NMR (400 MHz, CDCl₃) δ 7.86 (dd, *J* = 5.4, 3.1 Hz, 2H, H-1), 7.73 (dd, *J* = 5.4, 3.1 Hz, 2H, H-1'), 6.79 – 6.62

(m, 3H, H-2 and 3), 4.19 – 4.12 (m, 1H, H-5), 3.91 (d, $J = 5.2$ Hz, 2H, H-6 and 6'), 3.27 (dd, $J = 13.1, 4.6$ Hz, 1H, H-7), 3.16 (dd, $J = 13.1, 7.0$ Hz, 1H, H-7'). ^{13}C NMR (100 MHz, CDCl_3) δ 169.1 (C=O), 150.1 (d, $J = 7.5$ Hz, 1C, Ar-F), 134.4 (dd, $J = 26.9, 4.3$ Hz, 1C, Ar), 132.9 (C-1), 131.8 (C-1a), 123.6 (C-1'), 112.7 (dd, $J = 27.1, 3.8$ Hz, 1C, Ar), 110.7 (Ar), 103.9 (Ar) 69.0 (C-7), 47.7 (C-5), 42.1 (C-6). HRMS calcd. (M+H) for $\text{C}_{17}\text{H}_{14}\text{F}_2\text{N}_2\text{O}_3$ 333.1045; found 333.1039.

Biology

Evaluation of *in vitro* cytotoxicity

A simple MTT (3-(4,5-dimethylthiazolyl-2)-2,5-diphenyltetrazolium bromide) assay was used to determine the *in vitro* cytotoxicity of synthesized compounds against the HepG2 cell line.^{37,38} HepG2 cells were grown in culture flasks with DMEM media supplemented with 10% FBS and gentamicin at 37°C and 5% CO_2 , with media changes three times a week. The cells were then trypsinized, washed, and resuspended in a complete medium before being divided into 96-well plates with 5000 cells per well and incubated for 24 hours at 37°C. After 48 hours of incubation, the supernatant was removed, and 100 μL of MTS solution in full DMEM was added to each well. The plates were then incubated for 2 hours at 37°C and examined in a spectrophotometer using absorbance measurement at 450 nm. The obtained data were analyzed in Excel to evaluate cytotoxicity.

In vitro Parasite cultivation

Pf3D7 was cultured, applying the techniques outlined by Trager and Jensen.³⁹ A complete medium consisting of RPMI 1640, 0.2% NaHCO_3 , and 0.5% AlbuMax II, supplemented with 0.1 mM hypoxanthine and 25 mg/mL gentamicin, was utilized for the cultivation of parasites in human O+ red blood cells. The parasites were cultured under controlled conditions of a gas composition consisting of 5% oxygen, 5% carbon dioxide, and 90% nitrogen while being kept at a temperature of 37°C. The Giemsa-stained blood method was used to monitor the morphology of the parasite. The culture was synchronized through the application of Sorbitol treatment.⁴⁰

Antiplasmodial activity evaluation

The study conducted parasite growth inhibition assays on synchronized parasites cultured in sterile 96-well plates. The total volume per well was 100 μL , with an initial parasitemia of 0.5% and a hematocrit of 2%. The plates were introduced into a sealed chamber, purged with a gaseous mixture of 5% oxygen, 5% carbon dioxide, and 90% nitrogen, and left undisturbed for 48 hours. Following a 48-hour incubation period, a SYBR Green solution consisting of 100 μL of 0.2 μL SYBR Green per mL lysis buffer was introduced into each well. The plates were then stirred in a lightless environment at ambient temperature for 1 hour. Subsequently, fluorescence was recorded in a Multimode microplate reader by exciting the sample at 490 nm and detecting the emission at 530 nm. The IC_{50} values were determined by normalizing fluorescent counts and subjecting them to nonlinear least square regression using PrismTM software. IC_{50} values were determined by plotting dose-dependent curves.

Haemolysis assay

The hemolysis assay suspended red blood cells (RBCs) at a concentration of 10% (v/v). Before the assay, the RBCs were washed with PBS (pH 7.4) and resuspended in PBS. Afterward, the erythrocytes were subjected to varying concentrations of compounds for 2 hours at a temperature of 37 °C. Following the treatment, the samples underwent centrifugation at 800 revolutions per minute for 5 minutes while maintained at ambient temperature. The liquid portion of the sample was gathered and subjected to spectrophotometric analysis at a wavelength of 540 nm to ascertain the degree of erythrocyte hemolysis.

Time-dependent and stage-specific assay

After the progression assay, Time-dependent and blood-stage-specific assessment effects were estimated for potent compounds on *Pf3D7*. In short, ring-stage parasites of synchronized culture (1.1% parasitemia and 4% hematocrit) were treated with the most active compound **3f** at IC_{50} concentration. Parasite culture was incubated at 37 °C and monitored from 3h to 48h in the complete culture medium. For various time points, the parasitemia changes were measured with the help of a bright field microscope (Nikon), and the morphological changes in the parasite were carried out by counting the Giemsa-stained slides.

Computational studies

SWISS ADME⁴¹ and Molsoft L.L.C.³¹ were used to calculate the ADME profile of all the designed and synthesized compounds. The predicted ADME properties include Molecular weight, H-bond acceptor, H-bond donors, Predicted octanol/water partition coefficient (MLogP), TPSA (Total Polar Surface Area), Lipinski violation, Drug-likeness score, and BBB value. The methodology followed for molecular docking and MD simulation analysis is described in supporting information.⁴² The computational work was performed using Schrödinger software (release 2020-1; License: Hansraj College, University of Delhi #35125).

CONCLUSION

Given the existing difficulties associated with current treatment approaches, there is a pressing need to create innovative pharmaceutical therapies with broad-spectrum antiparasitic activities that specifically address malaria and schistosomiasis. Due to the significant impact of parasitic diseases on human populations, developing novel therapeutics is an urgent and crucial undertaking, particularly in developing countries. Novel 16 Pht-HEA analogs were synthesized in good to fair yield using slightly modified methods under microwave irradiation. Phenotypic screening of the compounds led to a hit compound **3f** against *Pf3D7* without any cytotoxic indications upto 500 μM concentration. Molecular modeling and MD simulation studies for the hit **3f** against various essential *Pf* proteins indicated that aminopeptidase N could be a target. However, the computational results need to be validated through enzymatic assays. Our study highlights the potential of Pht and HEA-based analogs as antimalarial agents. It provides a starting point for further optimizing and developing these compounds as potential drug candidates.

ACKNOWLEDGMENTS

BR thanks the Science & Engineering Research Board for the financial support (CRG/2020/005800) for financial support. We acknowledge Dr. Agam P. Singh's constant support while doing cell-based assays in his laboratory. Dr. Prem Prakash Sharma is acknowledged for his assistance in performing *in silico* studies. MB is grateful to ICMR for the senior research fellowship.

SUPPLEMENTARY INFORMATION

¹H NMR, ¹³C NMR, ADME calculations, HPLC Purity, cytotoxicity, hemolysis, computational details of protein target used for docking.

Conflict of interest: Authors declare no conflict of interest.

REFERENCES AND NOTES

- M.C. Thomson, L.R. Stanberry. Climate Change and Vectorborne Diseases. *New England Journal of Medicine* 2022, 387 (21), 1969–1978.
- A. Daina, O. Michielin, V. Zoete. SwissADME: a free web tool to evaluate pharmacokinetics, drug-likeness and medicinal chemistry friendliness of small molecules. *Scientific Reports* 2017 7:1 2017, 7 (1), 1–13.
- I.U. Ogbuanu, K. Otieno, R. Varo, et al. Burden of child mortality from malaria in high endemic areas: Results from the CHAMPS network using minimally invasive tissue sampling. *Journal of Infection* 2024, 88 (3), 106107.
- P.R. Torgerson, B. Devleeschauwer, N. Praet, et al. World Health Organization Estimates of the Global and Regional Disease Burden of 11 Foodborne Parasitic Diseases, 2010: A Data Synthesis. *PLoS Med* 2015, 12 (12), e1001920.
- C. Upadhyay, M. Chaudhary, R.N. De Oliveira, et al. Fluorinated scaffolds for antimalarial drug discovery. *Expert Opin Drug Discov* 2020, 15 (6), 705–718.
- C. Barillas-Mury, J.M.C. Ribeiro, J.G. Valenzuela. Understanding pathogen survival and transmission by arthropod vectors to prevent human disease. *Science* (1979) 2022, 377 (6614).
- World malaria report 2023 <https://www.who.int/teams/global-malaria-programme/reports/world-malaria-report-2023> (accessed Oct 30, 2024).
- V. Reddy, D.J. Weiss, J. Rozier, F.O. ter Kuile, S. Dellicour. Global estimates of the number of pregnancies at risk of malaria from 2007 to 2020: a demographic study. *Lancet Glob Health* 2023, 11 (1), e40–e47.
- D.M. Parente, J. Morton. Role of the Pharmacist in Antimicrobial Stewardship. *Medical Clinics of North America* 2018, 102 (5), 929–936.
- R.T. Eastman, D.A. Fidock. Artemisinin-based combination therapies: a vital tool in efforts to eliminate malaria. *Nature Reviews Microbiology* 2009 7:12 2009, 7 (12), 864–874.
- D.J. Weiss, T.C.D. Lucas, M. Nguyen, et al. Mapping the global prevalence, incidence, and mortality of *Plasmodium falciparum*, 2000–17: a spatial and temporal modelling study. *The Lancet* 2019, 394 (10195), 322–331.
- K.J. McLean, J. Straimer, C.S. Hopp, et al. Generation of Transmission-Competent Human Malaria Parasites with Chromosomally-Integrated Fluorescent Reporters. *Scientific Reports* 2019 9:1 2019, 9 (1), 1–10.
- L.S. Ross, D.A. Fidock. Elucidating Mechanisms of Drug-Resistant *Plasmodium falciparum*. *Cell Host Microbe* 2019, 26 (1), 35–47.
- M.B. Laurens. RTS,S/AS01 vaccine (Mosquirix™): an overview. *Hum Vaccin Immunother* 2020.
- S. Singh, N. El-sakkary, D.E. Skinner, et al. Synthesis and Bioactivity of Phthalimide Analogs as Potential Drugs to Treat Schistosomiasis, a Neglected Disease of Poverty. *Pharmaceuticals* 2020, 13 (2), 25.
- V. Singh, R.S. Hada, R. Jain, et al. Designing and development of phthalimides as potent anti-tubulin hybrid molecules against malaria. *Eur J Med Chem* 2022, 239, 114534.
- A.C.L. Leite, J.W.P. Espíndola, M.V. de O. Cardoso, G.B. de O. Filho. Privileged Structures in the Design of Potential Drug Candidates for Neglected Diseases. *Curr Med Chem* 2019, 26 (23), 4323–4354.
- P.S. Phatak, R.D. Bakale, S.T. Dhumal, et al. Synthesis, antitubercular evaluation and molecular docking studies of phthalimide bearing 1,2,3-triazoles. *Synth Commun* 2019, 49 (16), 2017–2028.
- S.S. Hamdani, B.A. Khan, S. Hameed, et al. Synthesis and evaluation of novel S-benzyl- and S-alkylphthalimide-oxadiazole-benzenesulfonamide hybrids as inhibitors of dengue virus protease. *Bioorg Chem* 2020, 96, 103567.
- Shalini, S. Kumar, M. Gendrot, et al. Amide Tethered 4-Aminoquinoline-naphthalimide Hybrids: A New Class of Possible Dual Function Antiplasmodials. *ACS Med Chem Lett* 2020, 11 (12), 2544–2552.
- Shalini, J. Legac, A.A. Adeniyi, et al. Functionalized Naphthalimide-4-aminoquinoline Conjugates as Promising Antiplasmodials, with Mechanistic Insights. *ACS Med Chem Lett* 2020, 11 (2), 154–161.
- Shalini, M.D. Johansen, L. Kremer, V. Kumar. Variedly connected 1,8-naphthalimide-7-chloroquinoline conjugates: Synthesis, anti-mycobacterial and cytotoxic evaluation. *Bioorg Chem* 2019, 92, 103241.
- A. Rani, A. Sharma, J. Legac, et al. A trio of quinoline-isoniazid-phthalimide with promising antiplasmodial potential: Synthesis, in-vitro evaluation and heme-polymerization inhibition studies. *Bioorg Med Chem* 2021, 39, 116159.
- A. Rani, A. Singh, J. Gut, P.J. Rosenthal, V. Kumar. Microwave-promoted facile access to 4-aminoquinoline-phthalimides: Synthesis and anti-plasmodial evaluation. *Eur J Med Chem* 2018, 143, 150–156.
- M. Henary, C. Kananda, L. Rotolo, et al. Benefits and applications of microwave-assisted synthesis of nitrogen containing heterocycles in medicinal chemistry. *RSC Adv* 2020, 10 (24), 14170–14197.
- K. Martina, G. Cravotto, R.S. Varma. Impact of Microwaves on Organic Synthesis and Strategies toward Flow Processes and Scaling up. *Journal of Organic Chemistry* 2021, 86 (20), 13857–13872.
- S. Kumar, C. Upadhyay, M. Bansal, et al. Experimental and Computational Studies of Microwave-Assisted, Facile Ring Opening of Epoxide with Less Reactive Aromatic Amines in Nitromethane. *ACS Omega* 2020, 5 (30), 18746–18757.
- S. Singh, V. Rajendran, J. He, et al. Fast-Acting Small Molecules Targeting Malarial Aspartyl Proteases, Plasmepsins, Inhibit Malaria Infection at Multiple Life Stages. *ACS Infect Dis* 2019, 5 (2), 184–198.
- A. Kumar Singh, V. Rajendran, S. Singh, et al. Antiplasmodial activity of hydroxyethylamine analogs: Synthesis, biological activity and structure activity relationship of plasmepsin inhibitors. *Bioorg Med Chem* 2018, 26 (13), 3837–3844.
- A.K. Singh, S. Rathore, Y. Tang, et al. Hydroxyethylamine Based Phthalimides as New Class of Plasmepsin Hits: Design, Synthesis and Antimalarial Evaluation. *PLoS One* 2015, 10 (10), e0139347.
- M. Gupta, H.J. Lee, C.J. Barden, D.F. Weaver. The Blood-Brain Barrier (BBB) Score. *J Med Chem* 2019, 62 (21), 9824–9836.
- R.G.R.J.D.P. Madhusudhan G. A facile synthesis of 2-((5R)-2-oxo-5-oxazolidinyl)methyl)-1H-isoindole-1,3(2H)-dione. *Indian J Chem* 2006, 45B, 1264–1268.
- F. Ding, N. V. Dokholyan. Emergence of Protein Fold Families through Rational Design. *PLoS Comput Biol* 2006, 2 (7), e85.
- P. Pino, R. Caldelari, B. Mukherjee, et al. A multistage antimalarial targets the plasmepsins IX and X essential for invasion and egress. *Science* (1979) 2017, 358 (6362), 522–528.
- P.P. Sharma, S. Kumar, S. Srivastava, et al. Computational study of novel inhibitory molecule, 1-(4-((2S,3S)-3-amino-2-hydroxy-4-phenylbutyl)piperazin-1-yl)-3-phenylurea, with high potential to competitively block ATP binding to the RNA dependent RNA polymerase of SARS-CoV-2 virus. *J Biomol Struct Dyn* 2022, 40 (20), 10162–10180.

36. P.P. Sharma, S. Kumar, K. Kaushik, et al. In silico validation of novel inhibitors of malarial aspartyl protease, plasmepsin V and antimalarial efficacy prediction. *J Biomol Struct Dyn* 2022, 40 (18), 8352–8364.
37. C. Upadhyay, S. Bhattacharya, S. Kumar, et al. Novel fluorinated piperazine based-amino acid derivatives as antiplasmodial agents: Synthesis, bioactivity and computational studies. *Chemical Biology Letters* 2023, 10 (3), 543.
38. S. Kumar, D. Kumar, C. Upadhyay, et al. Functionalization of cellulose nanocrystals with a potent antimalarial compound: Synthesis, characterization, and biological studies. *Int J Biol Macromol* 2024, 282, 136660.
39. W. Trager, J.B. Jensen. Human Malaria Parasites in Continuous Culture. *Science (1979)* 1976, 193 (4254), 673–675.
40. C. Upadhyay, N. Sharma, S. Kumar, et al. Synthesis of the new analogs of morpholine and their antiplasmodial evaluation against the human malaria parasite *Plasmodium falciparum*. *New Journal of Chemistry* 2021, 46 (1), 250–262.
41. A. Daina, O. Michielin, V. Zoete. SwissADME: a free web tool to evaluate pharmacokinetics, drug-likeness and medicinal chemistry friendliness of small molecules. *Scientific Reports* 2017 7:1 2017, 7 (1), 1–13.
42. M. Bansal, S. Kumar, B. Rathi. Synthesis of novel phthalimide-based piperazine conjugated analogs as anti-malarial agents. *Chemical Biology Letters* 2023, 10 (4), 627.